CrystEngComm

Accepted Manuscript

ROYAL SOCIETY OF CHEMISTRY

www.rsc.org/crystengcomm

Journal Name

ARTICLE

Ambient Synthesis of a Multifunctional 1D/2D Hierarchical Ag-Ag_2S Nanowire/Nanosheet Heterostructure with Diverse Applications

Received 00th January 20xx,
Accepted 00th January 20xx

DOI: 10.1039/x0xx00000x

www.rsc.org/

Jinyan Xiong,[a] Chao Han,[a] Weijie Li,[a] Qiao Sun,[b] Jun Chen,[c] Shulei Chou,[a] Zhen Li,[a,b]* and Shixue Dou [a]

A new type of unique 1D/2D hierarchical Ag-Ag_2S heterostructures is fabricated by an extremely simple solution route under ambient conditions. The morphology, size, crystal structure and composition of the products were comprehensively investigated, and it was found the reaction time and the amount of S powder play crucial roles in the formation of well-defined 1D/2D hierarchical Ag-Ag_2S heterostructures. The diffusion and Ostwald ripening processes dominate the evolution of the heterostructure. The resultant 1D/2D Ag-Ag_2S hybrids exhibit great potential in Li/Na ions battery anodes, SERS detection and decoloration towards organic dyes.

Introduction

Semiconductor-noble metal-based hybrid nanostructures have promising potential in energy, environmental, and catalysis applications, due to their unique optical, electrical, catalytic properties arising from each component and their synergistic interactions.[1] Their great potential drives engineering nanofabrication and property of such semiconductor-metal hybrid nanomaterials with different architectures.[2] Being one of important semiconductor-noble metal hybrids, Ag-Ag_2S with different heterostructures, including nanotubes,[1a] nanowires,[3] nanoprisms,[4] and nanoparticles,[5] have been widely exploited in the past several years. It was reported that Ag-Ag_2S nanohybrids showed excellent properties in resistive switches,[3, 6] DNA hybridization probes,[4b] bactericidal effects,[4a, 5a, 7] photodegradation of pollutants,[1a, 5b] and water splitting.[6a] From the fabrication perspective, most fabrications of Ag-Ag_2S hybrids suffered from the drawbacks of high temperature,[5b] complicated processes,[6a, 7] and high energy consumption,[3] which seriously restrict their development and practical applications. It still remains a challenging but exciting topic to explore a facile strategy to prepare well-defined and unique multidimensional Ag-Ag_2S heterostructures, as well as to investigate their novel properties and potential applications.

Generally, the composition and structure of the hybrids play the pivotal role in determining their functions and applications.[8] Recent advances demonstrate that complex one-dimensional/two-dimensional (1D/2D) heterostructures composed of 1D nanowires and 2D nanosheets exhibit great potential in photocatalysis,[9] energy storage,[10] counter electrodes,[11] and photoelectrochemical cells,[12] owing to their unique structural features, which allows it to transport charge carriers very well along the axial direction and has relatively large surface area. However, to the best of our knowledge, there are sparse reports on preparation of 1D/2D Ag-Ag_2S heterostructures and exploration of their fascinating properties. Herein, a new type of 1D/2D Ag-Ag_2S architecture has been fabricated by an extremely simple solution route under ambient conditions, and the as-synthesized Ag-Ag_2S hybrids exhibit favorable multifunctional properties for energy and environmental applications.

Experimental

Experimental Methods

Ag nanowires (Ag NWs) were prepared according to our previous report with a minor modification.[13] In a typical synthesis, 10 mL of 1,2-propanediol containing PVP40 was loaded into a 25 mL vial, and heated with magnetic stirring in an oil bath at 135 °C for 1 h. 1 mL of NaCl in 1,2-propanediol solution (1 mM) was then quickly added, and stirring for another 5 min. Finally, $AgNO_3$ (0.1 M solution in 1,2-propanediol) was added to the mixture. The mixture solution

[a] Institute for Superconducting & Electronic Materials, The University of Wollongong, NSW 2500, Australia.
[b] School of Radiation Medicine and Radiation Protection, Collaborative Innovation Center of Radiation Medicine of Jiangsu Higher Education Institutions, Soochow University, 199 Ren Ai Road, Suzhou Industrial Park, Suzhou 215123, China.
[c] Intelligent Polymer Research Institute, The University of Wollongong, NSW 2500, Australia.

Electronic Supplementary Information (ESI) available: EDX spectrum and SEM image of as-synthesized 1D/2D Ag-Ag_2S heterostructures; TEM image and HRTEM image of the product prepared with an S to Ag ratio of 0.2:1; XRD patterns of the products prepared with different molar ratios of sulfur powder to Ag nanowires; SEM images and XRD pattern of the Ag-Ag_2S heterostructures obtained after 6 days; XRD pattern and SEM images of the Ag-Ag_2S nanoparticles and pure Ag_2S nanoparticles; SERS spectra of MB solutions with different concentrations adsorbed on 1D/2D hierarchical Ag-Ag_2S hybrid heterostructures. See DOI: 10.1039/x0xx00000x

was then heated at 135 °C with magnetic stirring for 1 h, yielding the gray Ag NWs.

Ag nanoparticles (Ag NPs) were prepared by the similar procedure applied to Ag NWs, except without NaCl.

1D/2D Ag-Ag_2S hierarchical heterostructures were prepared from the above synthesized Ag nanowires and sulphur powder. 8 mL freshly prepared Ag NW solution was firstly added into 10 mL ethanol under constant magnetic stirring for 10 min. Then, 0.0048 g sulfur powder was added into the reaction mixture. The reaction mixture was stirred for 24 h, and then the resultant Ag-Ag_2S precipitate was separated by centrifugation, washed with de-ionized water and absolute ethanol several times to remove impurities, and then dried at 60 °C.

Ag-Ag_2S heteronanoparticles were prepared using the similar approach to 1D/2D Ag-Ag_2S hierarchical heterostructures, except 8 mL of Ag NPs solution was added rather than Ag NWs solution.

Pure Ag_2S nanospheres were prepared from $AgNO_3$ and saturated Na_2S solution in ethanol in the presence of PVP. The reaction mixture was stirred for 24 h.

Characterization

The X-ray diffraction (XRD) measurements were performed on a GBC MMA X-ray diffractometer using Cu Kα1 radiation (40 kV). The XRD patterns were recorded from 20° to 80° with a scanning rate of 4°/min. SEM images were collected using a field-emission scanning electron microscope (JSM-7500FA, JEOL) operated at an accelerating voltage of 5 kV. TEM images were collected on a field-emission transmission electron microscope (ARM-200F, JEOL), using an accelerating voltage of 200 kV. Ultraviolet/visible (UV/vis) absorption spectra were recorded at room temperature on a UV-3600 (Shimadzu) spectrometer.

SERS measurement

2 mg as-synthesized 1D/2D Ag-Ag_2S hierarchical heterostructures were added into 200 μL of MB solution with a concentration of 10^{-3}, 10^{-4}, 10^{-5}, and 10^{-6} M, respectively. The mixture was ultrasonically dispersed for 10 min and shaken for 12 h in the dark at room temperature. Then, the dispersion was dropped onto a glass slide for the SERS measurement. All SERS spectra were collected on a JY HR 800 Raman spectrometer under excitation of 632 nm with a power of 13.5 mW.

Battery performance measurements

The electrode slurry for lithium/sodium ion batteries was prepared by mixing 70 wt% active powder material, 15 wt% carbon black, and 15 wt% carboxymethyl cellulose (CMC) binder. The slurry was pasted on copper foil, followed by drying in a vacuum oven overnight at 80 °C, and then pressing at a pressure of 30 MPa to enhance the contact between the mixture and the copper foil. For the lithium ion battery test, lithium foil was employed as both reference and counter electrode. The electrolyte was 1 M LiPF6 in an ethylene carbonate (EC)–diethyl carbonate (DEC) solution (1:1 v/v). For the sodium ion battery test, sodium foil was cut by the doctor blade technique from bulk sodium stored in mineral oil, which then was employed as both reference and counter electrode. The electrolyte was 1 M $NaClO_4$ in an EC/DEC solution (1:1 v/v). The cells were assembled in an argon-filled glove box, and their electrochemical performance was tested with a Land Test System in the voltage range of 0-2.5 V with a current density of 30 mA g^{-1}.

Decoloration test

The application of as-synthesized 1D/2D Ag-Ag_2S hierarchical heterostructures for decoloration of organic dyes was evaluated in both a dark environment and under solar light irradiation. In the experiment, 50 mg of the heterostructures were added into 50 mL of MB solution (10^{-5} M) at room temperature. After ultrasonic dispersion, the suspension was stirred in the dark for 30 min to ensure the establishment of an adsorption-desorption equilibrium between the hybrid structures and the MB. Then, the solution was exposed to irradiation of a LSC-100 Solar Simulator (Newport) under magnetic stirring. At each irradiation time interval, 2 mL of the suspension was collected and then centrifuged to remove the photocatalysts. The concentration of MB was analyzed by a Shimadzu UV-3600 spectrophotometer, and the characteristic absorption of MB at 664 nm was used to evaluate the decoloration activity. All of the measurements were carried out at room temperature.

Results and discussion

A typical Ag-Ag_2S architecture is synthesized through the reaction of Ag nanowires (NWs) with sulfur powder in ethanol at room temperature. The X-ray diffraction (XRD) pattern of the as-prepared sample in Fig. 1A indicates that the product is a hybrid consisting of monoclinic Ag_2S (JCPDS card No. 14-0072) and face-centered cubic Ag (JCPDS card No. 04-0783). The absence of impurity peaks in the XRD pattern suggests the high purity of the Ag-Ag_2S hybrid synthesized by this facile approach. The energy-dispersive X-ray (EDX) analysis result shown in Fig. S1 in the Electronic Supporting Information (ESI) indicates that the as-prepared hybrid is composed of Ag and S with an atomic ratio (i.e. Ag/S) higher than the stoichiometric ratio of 2:1 for Ag_2S, demonstrating the successful synthesis of the Ag-Ag_2S hybrid.

Characterizations by scanning electron microscopy (SEM) and transmission electron microscopy (TEM) provide insight into the morphology and detailed structure of the as-prepared Ag-Ag_2S hybrid. A panoramic view of the as-prepared sample shows uniform nanowires ~100 nm in diameter and several micrometers in length (Fig. S2). The enlarged SEM image in Fig. 1B reveals that many sheet-like nanostructures (~15 nm in thickness) have densely grown on the entire surface of the 1D nanowire to form a 1D/2D hierarchical nanostructure. Fig. 1C clearly shows a TEM image of an individual 1D/2D Ag-Ag_2S hierarchical nanostructure, in which sheet-like leaves surround 1D nanowire in a three-dimensional (3D) manner. The hybrid

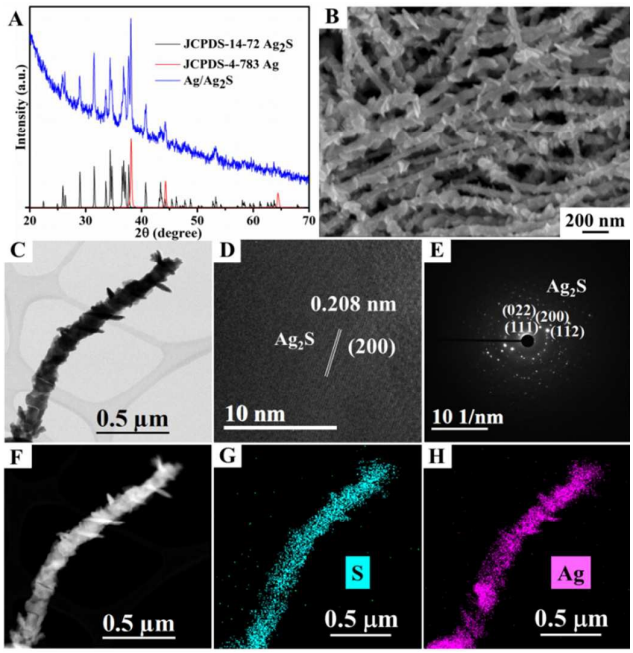

Fig. 1 (A) XRD pattern and (B) SEM image of the as-prepared Ag_2S-Ag heterostructures with the S/Ag ratio of 1:2; (C) TEM image, (D) HRTEM image, (E) SAED pattern, (F) HAADF image, and (G, H) corresponding EDX elemental mapping analysis of an individual Ag-Ag_2S heterostructure.

has two kinds of segments with different contrasts, in which the darker segment is metallic Ag and the brighter segment should be semiconducting Ag_2S. The high-resolution TEM (HRTEM) image in Fig. 1D shows a lattice fringe of 0.208 nm, which corresponds to the (200) planes of monoclinic Ag_2S. The selected area electron diffraction (SAED) pattern (Fig. 1E) also reveals the presence of Ag_2S in the hybrid. High-angle annular dark-field (HAADF) imaging was used to identify each chemical component. Due to the differences between Ag and S in scattering electrons, the as-prepared Ag-Ag_2S hybrid has different contrasts in the HAADF image (Fig. 1F), which is opposite to those observed in the bright field image, i.e. the bright segments indicate the presence of the heavier metal Ag, and the dark parts indicate the presence of Ag_2S. Elemental mapping of a single 1D/2D heterostructure obtained by HAADF-TEM reveals the homogeneous distribution of Ag and S elements in the hybrid (Fig. 1G and 1H).

The above results demonstrate the successful synthesis of 1D/2D Ag-Ag_2S hierarchical heterostructures. To understand the formation mechanism of such an interesting structure, we carried out time-dependent experiments and collected samples at different time intervals. The morphological and structural evolution of the products obtained with different reaction times were examined by SEM (Fig. 2). Before the addition of S powder, the Ag NWs are very straight, and the surfaces are very smooth (Fig. 2A). After addition of S powder and reaction for 30 min, no significant difference was observed on the surfaces of the Ag NWs at this early stage (Fig. 2B), although the reaction mixture changed from grey to yellow

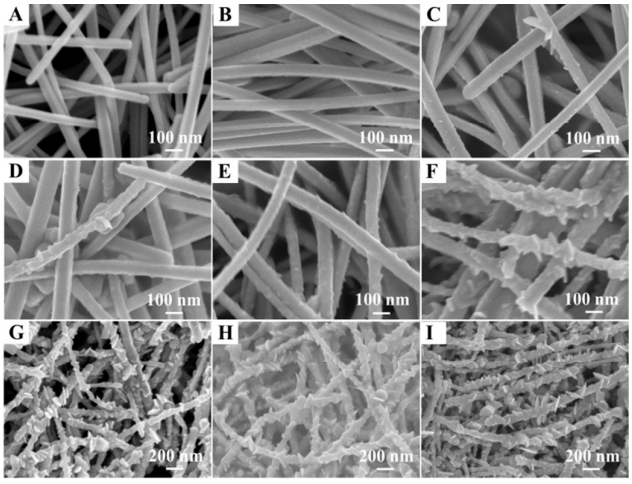

Fig. 2 SEM images of the products obtained with the S/Ag ratio of 1:2 at different reaction times: (A) 0 min, (B) 30 min, (C) 1.5 h, (D) 2 h, (E) 4 h, (F) 6 h, (G) 8 h, (H) 12 h, and (I) 24 h.

due to the formation of a thin Ag_2S layer on the surfaces of the NWs. As the reaction proceeded for 1.5 – 4 h, the surfaces of the nanowires became rougher, and a few spiny or scaly structures were formed, as shown in Fig. 2(C-E). The epitaxial growth of the Ag_2S nanostructures could be due to the excessive crystallization of Ag_2S in some places on the surface of the nanowire. When the reaction time was lengthened to 6 – 8 h, more and more quasi-nanosheets were formed on the nanowires to form a mace-like structure, as shown in Fig. 2(F-G). With further extended reaction time, the nanosheets adhering to the nanowires became larger and became joined to one another (Fig. 2H). After reaction for 24 h, the final products were entirely composed of the 1D/2D hybrid heterostructures (Fig. 2I).

These structures and morphologies were further analyzed by TEM and high-resolution TEM. As shown in Fig. 3A, the TEM images confirm that for the products obtained within 30 min, a thin Ag_2S layer is coated on the surface of the Ag NWs to form a well-defined core-shell Ag-Ag_2S nanowire with a relatively smooth surface, due to the sulfuration of the Ag NWs. The corresponding HRTEM image (Fig. 3B) clearly reveals that the resolved lattice fringes are 0.199 nm, corresponding to the *d*-spacing of the (-131) planes of monoclinic Ag_2S. With the growth of the Ag_2S shell, the surface of the hetero-nanowires became coarse [Fig. 3(C-D)]. Further prolonging the reaction time to 6 h led to the formation of a mace-like structure with a few quasi-nanosheets on the nanowires [Fig. 3(E-F)].

The crystalline structures and optical properties of above products were further studied and the results are shown in Fig. 4. The XRD patterns (Fig. 4A) clearly reveal that the intensity of the Ag_2S diffraction peaks are gradually increased with increasing reaction time, demonstrating the gradually formation of the Ag-Ag_2S hybrid and the increase content of Ag_2S. It is well known that Ag NWs show intense surface plasmon resonance (SPR) absorption in the visible region, which is highly sensitive to their diameter and length-to-

diameter ratio, as well as the optical and electronic properties of their surroundings.[13-14] The absorption spectra shown in Figure 4B were from ethanol-Ag and ethanol-Ag/Ag_2S dispersions collected at different reaction times, which were measured with a UV-3600 (Shimadzu) spectrometer in the UV-Vis-NIR region at room temperature. The scan speed is medium and the interval is 1 nm. The pure Ag NWs exhibit two absorbance peaks at 350 and 385 nm. The peak at 350 nm could be attributed to the longitudinal mode of the nanowires, which is similar to that of bulk Ag[14a, 15] or the out-of-plane quadrupole resonance of Ag NWs.[16] The peak at 385 nm is assigned to the transverse plasmon resonance of Ag NWs.[14a, 15] The optical response of the Ag NWs was observed to be markedly affected by the formation of Ag_2S. Upon the formation of the Ag_2S shell (30 min), the longitudinal mode almost disappeared and the transverse plasmon resonance of the Ag cores observed at about 385 nm decreased with redshifted and significantly broadened, which could possibly contributed to the synergistic effects between Ag NWs and Ag_2S shell in Ag-Ag_2S hybrids: the higher refractive index of Ag_2S (1.9-2.5)[17] than that of ethanol (~1.359)[14a, 18] and its high relative dielectric constant (ε_r= 6),[19] as well as the confinement of free electrons within the Ag core.[14a, 20] The peak width of SPR band increased slightly with increasing time (30 min-4 h), which implied that Ag nanowires are becoming more isolated with less and less electronic interactions between nearby unites. When the reaction time is 6 h, the spectra exhibited a new absorption band cantered around 495 nm and a very weak SPR peak. The new absorption is ascribed to the band gap of Ag_2S, which is similar to the reported absorption between 490-520 nm of rod-like Ag_2S nanocrystals,[21] 530 nm of Ag_2S nanofibers,[6c] 573 nm of Ag_2S nanotubes,[22] 443 nm of Ag_2S nanoparticle chains,[23] and 514-531 nm of the Ag_2S/Ag heterostructures.[7] The weak SPR observed herein indeed suggested that the good contact between the Ag_2S and Ag segments might ensure an effective charge transfer across the phase boundary, and the changes in the structure and shape of the product. When the time was increased to 8 h, the SPR absorption bands of Ag NWs almost disappeared owing to its further sulfuration, and the characteristic absorption feature of Ag_2S moved to the longer wavelength region at around 515 nm. The observed red-shifts may reflect the grain/crystallite growth of the Ag_2S and enlargement of the Ag_2S domains in the heterostructures. Eventually, with more and more quasi-nanosheets formed on the nanowires (see Fig. 2G and 2H), the characteristic absorption feature of Ag_2S moved to around 525 nm for the time at 12 h, providing strong evidence that essentially Ag NWs have turned into Ag-Ag_2S hybrid and the product mainly composed of Ag_2S component. The final dispersion was brownish black in appearance. The Ag-Ag_2S NWs obtained at 24 h exhibit similar absorption profile in comparison with the products obtained at 12 h, in which the characteristic absorption feature of Ag_2S remained at 525 nm and did not shift with increasing reaction time, due to the lack of obvious changes in the structures and shapes of final products (see Fig. 2I). Their broad absorbance from the UV to the near-infrared window is crucial for the full use of sunlight.

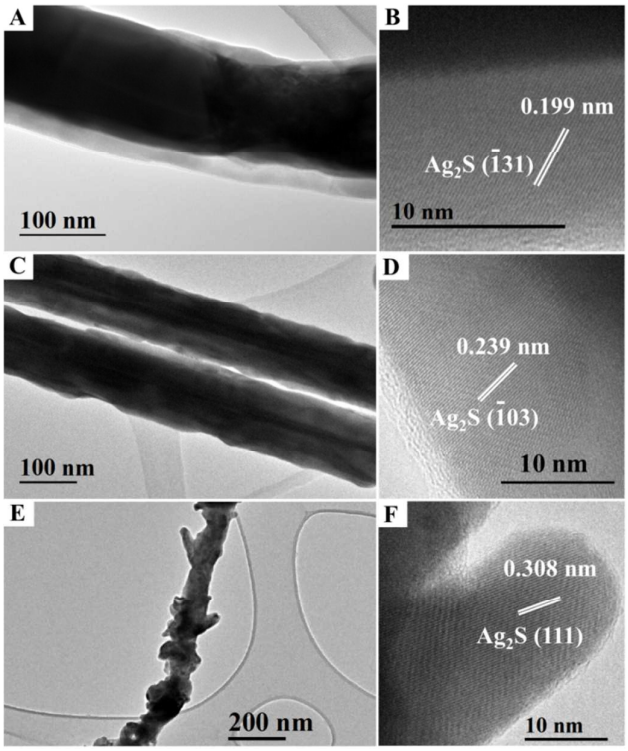

Fig. 3 TEM images (A, C, and E) and corresponding HRTEM images (B, D, and F) of the products obtained at different reaction times: (A, B) 30 min, (C, D) 4 h, and (E, F) 6 h.

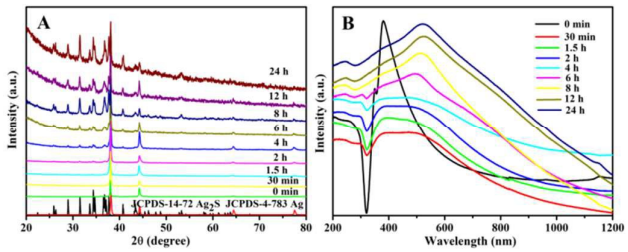

Fig. 4 (A) XRD patterns and (B) UV-Vis-NIR absorption spectra of the products obtained with the S/Ag ratio of 1:2 at different reaction times.

It should be noted that the formation of 1D/2D Ag-Ag_2S hierarchical heterostructures is strongly dependent on the Ag/S ratio. Fig. 5 presents SEM images of Ag-Ag_2S heterostructures obtained from different ratios of Ag/S after reaction for 24 h. The surfaces of heterostructures become smoother and smoother with the S/Ag ratio decreasing from 0.4:1 (Fig. 5A), through 0.33:1 (Fig. 5B) and 0.22:1 (Fig. 5C), to 0.2:1 (Fig. 5D). For the heterostructures obtained from the ratio of 0.2:1, the morphology of the initial Ag NWs remains almost unchanged, except for the formation of a thin Ag_2S layer on the surface of the Ag NWs, as shown by the TEM and HRTEM images in Fig. S3(A and B).

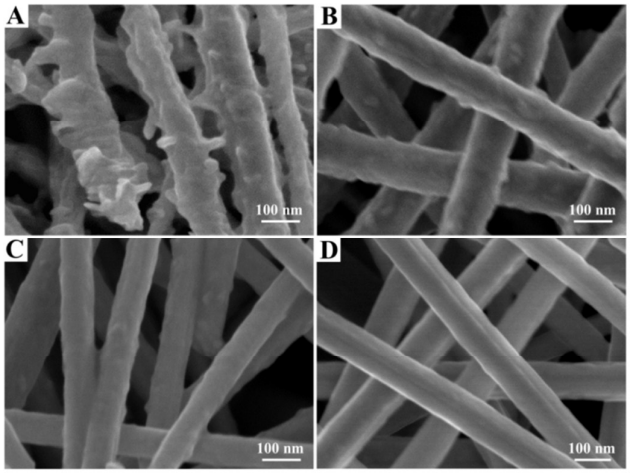

Fig. 5 SEM images of the products prepared with different molar ratios of sulfur powder to Ag nanowires: (A) 0.4:1, (B) 0.33:1, (C) 0.22:1, and (D) 0.2:1.

Based on these results, the formation of the 1D/2D Ag-Ag_2S hierarchical heterostructures can be illustrated in Scheme 1A, in which the diffusion and Ostwald ripening processes dominate the evolution of heterostructure morphology. It is well known that the room temperature diffusion of metals into semiconductors to form metal-semiconductor pairs generally occurs on the nanometer scale when the band-gap energy of the semiconductor is lower than about 2.5 eV.[2b, 24] The band gap of bulk Ag_2S crystal is about 0.9 eV at room temperature, and 1.4-2.3 eV for its nanoscale analogues.[2b, 7] Therefore, the diffusion of Ag metal in the Ag-Ag_2S nanowires well satisfies the aforementioned diffusion criterion. Scheme 1B shows a simplified diagram of energy level of Ag-Ag_2S nanocomposites, and the work function of Ag, the dominant energy level, the bottom of the conduction band and the top of the valence band of Ag_2S, which are -4.26eV, -3.63 eV, -4.42 eV and -5.32eV, respectively, from the vacuum energy level.[2b, 7, 25] In equilibrium, the Fermi levels of Ag and Ag_2S should be at the same level. According to the potential alignment, the electrons (majority carriers) can drift from the Fermi level of Ag to the Fermi level (E_F, which is approximately treated as the donor level) of the *n*-type Ag_2S semiconductor upon they are in contact, leaving some positive charge buildup on the metal contact interface,[7, 26] which could facilitate the diffusion of Ag in Ag_2S and result in substitutional interstitial processes.[25] As a consequence, the Ag-Ag_2S interface causes the bending and upshift of energy bands.[26] In the presence of S powder, which could serve as a strong oxidant, the surface reactive Ag atoms of the nanowires are oxidized to form a thin uniform Ag_2S layer at an early stage. The subsequent diffusion of Ag would continue, as well as its reaction with S at different sites, leading to the growth of convexity due to the increase in internal energy arising from the interfacial strain caused by the lattice mismatch between Ag and Ag_2S, and due to the large volume expansion during the sulfurization reaction, since the molar volumes of Ag and Ag_2S are 10.3 cm^3 mol^{-1} and 34.3 cm^3 mol^{-1}, respectively.[19a] The initially formed Ag_2S convexity continues its growth and undergoes an Ostwald ripening process to turn into nanosheets. With the growth of Ag_2S, the diffusion of Ag atoms from the internal Ag core to the surface Ag_2S becomes slower and slower, leading to negligible difference in the 1D/2D hybrid heterostructures obtained after 24 h. The SEM images and XRD pattern of a sample reacted for 6 days are shown in Fig. S4, which are similar to those obtained at 24 h. Compared to previously reported methods for the fabrication of 1D Ag-Ag_2S heterostructures, a major advantage of the present work is the use of stable sulfur powder rather than Na_2S to synthesize this new type of well-defined 1D/2D hybrid architecture under ambient conditions.[4b, 27]

As a proof-of-concept application of this intriguing hybrid nanostructure, the obtained 1D/2D hierarchical Ag-Ag_2S heterostructures were used as multifunctional materials in rechargeable Li/Na-ion batteries, in decolouration of organic dyes, as well as in surface-enhanced Raman spectroscopy (SERS) detection. Fig. 6A shows the cycling performance and coulombic efficiency of electrodes in Li-ion batteries fabricated from the 1D/2D hierarchical Ag-Ag_2S heterostructures. Their capacities drop in the first few cycles due to the formation of a solid electrolyte interphase (SEI) film, which is similar to what happens in other nanostructure based electrodes.[28] The first few cycles involve the formation of a stable SEI film resulting from the electrolyte decomposition, which degrades the capacity. The capacity slowly decreases to around 201 mAh g^{-1} after 25 cycles of charging and discharging, followed by a gradual increase to 302 mAh g^{-1} after 200 cycles. The increasing trend in the capacity is similar to that in the

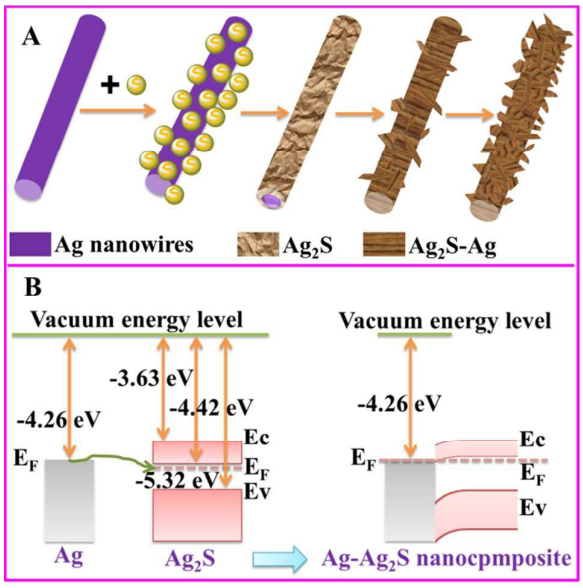

Scheme 1 (A) Schematic illustration of the synthesis of 1D/2D Ag-Ag_2S heterostructures and (B) Simplified band structures in Ag-Ag_2S system before and after contact.

reported literature, and the capacity is larger than that of pure Ag_2S nanoparticles.[29]

From the charge-discharge curves in Fig. 6B, the initial discharge and charge capacities are 885 and 626 mA h g^{-1}, respectively, corresponding to a coulombic efficiency of 71%, which is higher than that of the reported Ag_2S/C nanocomposite (~61%) and pure Ag_2S (~40%), and the charge capacity of the Ag-Ag_2S heterostructure electrode was also larger than for the other two.[29] Nevertheless, the coulombic efficiency increased to above 98% after 25 cycles, suggesting excellent retention capacity of the Ag-Ag_2S electrode with 1D/2D morphology. These electrochemical characteristics can be attributed to their composition and unique 1D/2D structure: (1) the Ag in the hybrid possesses much better electrical conductivity than the pure Ag_2S and provides interconnected charge pathways so that the conductivity and mechanical strength of the whole heterostructure electrode are improved; (2) the 1D nanowires with superior electronic conductivity and the 2D nanosheets effectively shorten the diffusion length of Li ions in the small primary subunits;[30] (3) the unique hierarchical 1D/2D structure could not only provide more sites or paths for lithium ion storage or transport, but also provides enough space to buffer the volume expansion during cycling and facilitate good contact with the conductive carbon black.[31]

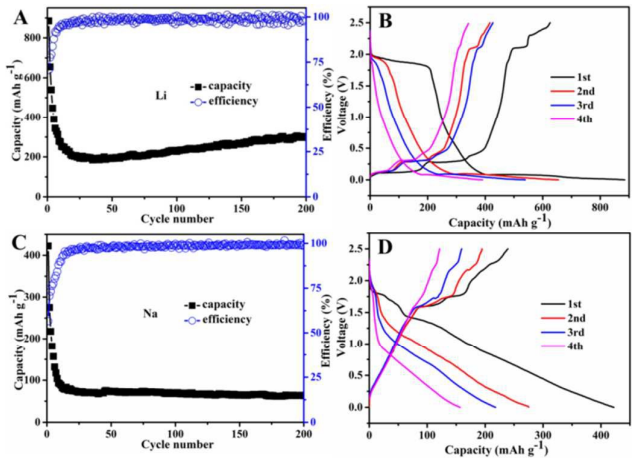

Fig. 6 Cycling performance and Charge-discharge voltage profiles for the first 4 cycles of the 1D/2D hierarchical Ag-Ag_2S heterostructure electrode used as anode for the lithium battery (A and B) and the sodium battery (C and D) at a specific current of 30 mA g^{-1}.

In addition to the lithium ion battery, the 1D/2D hierarchical Ag-Ag_2S heterostructure electrode was also used as anode for the sodium ion battery for the first time. As shown in Fig. 6C and Fig. 6D, its capacity decreased dramatically from 422 to 91 mAh g^{-1} in the first 10 cycles, followed by a gradual decrease to 63 mAh g^{-1} after 200 cycles. The initial discharge and charge capacities are 422 and 239 mA h g^{-1}, respectively, corresponding to a coulombic efficiency of 57%, and the coulombic efficiency increased to above 98% after 30 cycles, which also suggesting excellent capacity retention of the Ag-Ag_2S electrode with 1D/2D morphology.

Fig. 7A shows the removal of methylene blue (MB) by the 1D/2D Ag-Ag_2S hierarchical heterostructure under both visible light illumination and in dark conditions. Approximately 76% of the dye is decolorized under solar light exposure of 150 min as compared to the 69% efficiency in dark conditions, demonstrating the weak photocatalytic effect of the 1D/2D Ag-Ag_2S hierarchical heterostructures (Fig. 7B). It is also implied, however, that the adsorption process is quicker than the photodegradation process. Ag_2S works more as an adsorbent and less as a photosensitizer and electron donator in imparting the decoloration effects to the Ag NWs under solar light irradiation. The adsorption process transfers MB molecules to the photocatalyst surfaces, but the solar-light-driven photocatalysis process cannot radically eliminate the MB. Compared with Ag-Ag_2S nanoparticles (Fig. 7C and Fig. S5 in the Supporting information), pure Ag_2S nanoparticles (Fig. 7D and Fig. S6 in the Supporting information), and Ag NWs, the excellent decoloration of MB on the 1D/2D Ag-Ag_2S hierarchical heterostructures can be ascribed to their strong adsorption capability in the dark, due to the interfacial effect after introduction of Ag_2S nanosheets onto the surface of the Ag NWs, and the weak photodegradation of the adsorbed MB molecules through the heterostructures.

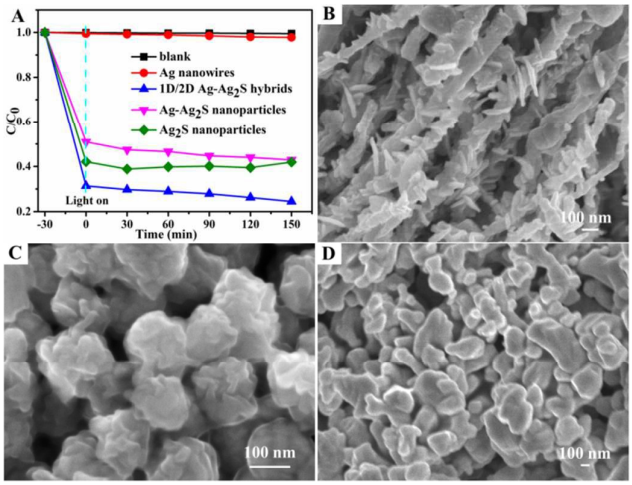

Fig. 7 (A) Decoloration activity of the 1D/2D hierarchical Ag-Ag_2S compared with Ag-Ag_2S nanoparticles and pure Ag_2S nanoparticles and SEM images of 1D/2D hierarchical Ag-Ag_2S (B), Ag-Ag_2S nanoparticles (C) and pure Ag_2S nanoparticles (D).

Surface-enhanced Raman scattering (SERS) spectroscopy is a powerful tool for detection of traces of chemical and biological species. To study the SERS responses of our as-prepared 1D/2D hierarchical Ag-Ag_2S heterostructures, the commonly used organic dye methylene blue (MB) was selected as a target molecule. The original Raman spectrum of MB is dominated by ν(C–C) ring stretching at 1622 cm^{-1}, α(C–H) in-plane ring deformation at 1398 cm^{-1}, and δ(C–N–C) skeletal deformation at 449 cm^{-1}.[32] Fig. 8 shows the Raman spectra of MB deposited on different glass slides coated with 1D/2D hierarchical Ag-Ag_2S nanowires, Ag-Ag_2S nanoparticles, and pure Ag_2S nanoparticles, in comparison with the spectrum of MB. It is obvious that most signals of the characteristic peaks were highly enhanced in the SERS spectra compared with that

of MB solution (10^{-3} M). The characteristic peaks of MB are located almost in the same place or only slightly shifted, which indicates the adsorption of MB on the substrate surface. According to the peak at 1626 cm^{-1}, the signal enhanced by the 1D/2D hierarchical Ag-Ag_2S heterostructures and the Ag-Ag_2S nanoparticles is higher than that from the pure Ag_2S nanoparticles, which demonstrates the significant role of Ag in the hybrid structure in enhancement. It is generally accepted that both electromagnetic enhancement and chemical enhancement could contribute to the overall surface enhancement.[33] The unique strong local plasmon resonance from the Ag metal in the hybrid structure generates more "hot spots" that can contribute to the SERS enhancement, compared to the pure Ag_2S nanoparticles.[34] The highest intensity in the case of the 1D/2D hierarchical Ag-Ag_2S heterostructures is probably due to the hierarchical and concave structures constructed from 1D nanowires and 2D nanosheets, which may boost their enhancement in comparison with spherical nanoparticles with smooth surfaces.[33, 35] The enhancement of pure Ag_2S nanoparticles is relatively weaker, since the localized surface plasmon

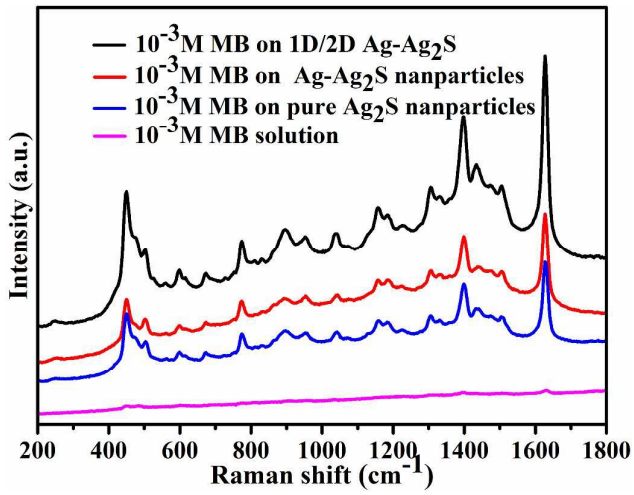

Fig. 8 SERS spectra of the 1D/2D hierarchical Ag-Ag_2S compared with Ag-Ag2S nanoparticles and pure Ag_2S nanoparticles.

resonance (LSPR) of Ag_2S is usually located in the near-infrared/infrared region, and the SERS enhancement mainly results from the charge transfer resonance between the Ag_2S and MB molecules.[4b, 33-34, 36]

In order to demonstrate the application of as-fabricated 1D/2D hierarchical Ag-Ag_2S as a promising SERS-active substrate, we also examined the dependence of SERS signal on the concentration of adsorbed MB (Fig. S7). The intensity of spectra increases with the increase of concentration from 10^{-6} M to 10^{-3} M. At low concentration (i.e.10^{-5}/10^{-6} M), the characteristic peaks of MB at 1622 cm^{-1}, 1398 cm^{-1} and 449 cm^{-1} are faintly visible, and they become much more prominent and sharp at higher concentration (i.e. 10^{-4} ~ 10^{-3} M). This result is probably due to more dye molecules adsorbed on the substrate surface, which can create more surface active "hot spots" compared to the lower concentrations.

Conclusions

In summary, unique 1D/2D hierarchical Ag-Ag_2S heterostructures were successfully prepared at room temperature by an extremely simple solution method. The growth of Ag-Ag_2S hybrids is dominated by the diffusion and Ostwald ripening processes. The resultant 1D/2D hierarchical Ag-Ag_2S heterostructures exhibit good capacity when used as Li/Na ions battery anodes, high sensitivity for detection of organic dyes through SERS, and decoloration activity towards organic dyes. It was expected that this work could open up new avenues towards the facile and rational synthesis of multifunctional 1D/2D hierarchical architectures of semiconductor-noble metal hybrids for diverse applications.

Acknowledgements

The authors gratefully acknowledge financial support from the Australian Research Council (ARC) through the Discovery Projects DP 130102274 and DP130102699. The authors would like to thank the support from ISEM at UOW, Jiangsu Provincial Key Laboratory of Radiation Medicine and Protection, the Priority Academic Program Development of Jiangsu Higher Education Institutions (PAPD) at Soochow University, and. The authors also acknowledge the use of the facilities in the UOW Electron Microscopy Centre (with particular thanks to Dr. David Mitchell), and Australian Nantional Fabrication Facility (ANFF)-Materials node for facility access. They also thank Dr. Tania Silver for critical reading of the manuscript.

Notes and references

1 (a) W. Yang, L. Zhang, Y. Hu, Y. Zhong, H. B. Wu and X. W. Lou, *Angew. Chem., Int. Ed.*, 2012, **51**, 11501; (b) S. T. Kochuveedu, Y. H. Jang and D. H. Kim, *Chem. Soc. Rev.*, 2013, **42**, 8467; (c) X. Huang, Z. Zeng, S. Bao, M. Wang, X. Qi, Z. Fan and H. Zhang, *Nat. Commun.*, 2013, **4**, 1444.

2 (a) W.-T. Chen, Y.-K. Lin, T.-T. Yang, Y.-C. Pu and Y.-J. Hsu, *Chem. Commun.*, 2013, **49**, 8486; (b) X. Hong, Z. Yin, Z. Fan, Y.-Y. Tay, J. Chen, Y. Du, C. Xue, H. Chen and H. Zhang, *Small*, 2014, **10**, 479; (c) Z. Fan, X. Zhang, J. Yang, X.-J. Wu, Z. Liu, W. Huang and H. Zhang, *J. Am. Chem. Soc.*, 2015, **137**, 10910.

3 G. R. Bourret and R. B. Lennox, *Nanoscale*, 2011, **3**, 1838.

4 (a) S. Xiong, B. Xi, K. Zhang, Y. Chen, J. Jiang, J. Hu and H. C. Zeng, *Sci. Rep.*, 2013, **3**, 2177; (b) B. Liu and Z. Ma, *Small*, 2011, **7**, 1587.

5 (a) X. Ma, Y. Zhao, X. Jiang, W. Liu, S. Liu and Z. Tang, *ChemPhysChem*, 2012, **13**, 2531; (b) F. Jiang, Q. Tian, M. Tang, Z. Chen, J. Yang and J. Hu, *CrystEngComm*, 2011, **13**, 7189.

6 (a) Y. Li, X. Ye, Y. Ma and L. Qi, *Small*, 2015, **11**, 1183; (b) C. Liang, K. Terabe, T. Hasegawa and M. Aono, *Nanotechnology*,

2007, **18**, 485202; (c) H. Wang and L. Qi, *Adv. Funct. Mater.*, 2008, **18**, 1249.

7 M. Pang, J. Hu and H. C. Zeng, *J. Am. Chem. Soc.*, 2010, **132**, 10771.

8 (a) J. Hu, A. Liu, H. Jin, D. Ma, D. Yin, P. Ling, S. Wang, Z. Lin and J. Wang, *J. Am. Chem. Soc.*, 2015, **137**, 11004; (b) C. Yuan, H. B. Wu, Y. Xie and X. W. Lou, *Angew. Chem., Int. Ed.*, 2014, **53**, 1488; (c) C. Lan, J. Gong and Y. Jiang, *J. Alloys Compd.*, 2013, **575**, 24; (d) C. Lan, J. Gong, Y. Jiang and Q. Ding, *CrystEngComm*, 2012, **14**, 8063.

9 W. Zhou, Z. Yin, Y. Du, X. Huang, Z. Zeng, Z. Fan, H. Liu, J. Wang and H. Zhang, *Small*, 2013, **9**, 140.

10 J. Liu, J. Jiang, C. Cheng, H. Li, J. Zhang, H. Gong and H. J. Fan, *Adv. Mater.*, 2011, **23**, 2076.

11 X. Q. Chen, Z. Li, Y. Bai, Q. Sun, L. Z. Wang and S. X. Dou, *Chem. Eur. J.*, 2015, **21**, 1055.

12 B. Xu, P. He, H. Liu, P. Wang, G. Zhou and X. Wang, *Angew. Chem., Int. Ed.*, 2014, **53**, 2339.

13 J. Xiong, Z. Li, J. Chen, S. Zhang, L. Wang and S. Dou, *ACS Appl. Mater. Interfaces*, 2014, **6**, 15716.

14 (a) P. Ramasamy, D.-M. Seo, S.-H. Kim and J. Kim, *J. Mater. Chem.*, 2012, **22**, 11651; (b) R. Jin, Y. Cao, C. A. Mirkin, K. L. Kelly, G. C. Schatz and J. G. Zheng, *Science*, 2001, **294**, 1901.

15 (a) Z. Wang, J. Liu, X. Chen, J. Wan and Y. Qian, *Chem. Eur. J.*, 2005, **11**, 160; (b) Y. Sun, B. Gates, B. Mayers and Y. Xia, *Nano Lett.*, 2002, **2**, 165.

16 (a) S. Chen and D. L. Carroll, *Nano Lett.*, 2002, **2**, 1003; (b) R. Jin, Y. Charles Cao, E. Hao, G. S. Metraux, G. C. Schatz and C. A. Mirkin, *Nature*, 2003, **425**, 487; (c) Y. Gao, L. Song, P. Jiang, L. F. Liu, X. Q. Yan, Z. P. Zhou, D. F. Liu, J. X. Wang, H. J. Yuan, Z. X. Zhang, X. W. Zhao, X. Y. Dou, W. Y. Zhou, G. Wang, S. S. Xie, H. Y. Chen and J. Q. Li, *J. Cryst. Growth*, 2005, **276**, 606.

17 (a) D. Okoli, G. Okeke and A. Ekpunobi, *Pac. J. Sci. Tech.*, 2010, **11**, 411; (b) Y.-T. Long and C. Jing, *Springer*, *Berlin Heidelberg,* 2014; (c) J. Zhu, Y. Shen, A. Xie and L. Zhu, *J. Mater. Chem.*, 2009, **19**, 8871.

18 T. Hirakawa and P. V. Kamat, *J. Am. Chem. Soc.*, 2005, **127**, 3928.

19 (a) J. Zeng, J. Tao, D. Su, Y. Zhu, D. Qin and Y. Xia, *Nano Lett.*, 2011, **11**, 3010; (b) S. Chang, Q. Li, X. Xiao, K. Y. Wong and T. Chen, *Energy Environ. Sci.*, 2012, **5**, 9444.

20 R. T. Tom, A. S. Nair, N. Singh, M. Aslam, C. L. Nagendra, R. Philip, K. Vijayamohanan and T. Pradeep, *Langmuir*, 2003, **19**, 3439.

21 Y. Zhao, D. Zhang, W. Shi and F. Wang, *Mater. Lett.*, 2007, **61**, 3232.

22 X. Fu, H. Zou and L. Zhou, *J. Nanosci. Nanotechnol.*, 2010, **10**, 5851.

23 D. Li, H.-Z. Xie, J.-K. Liu and C.-J. Duan, *J. Exp. Nanosci.*, 2011, **6**, 209.

24 (a) T. Mokari, A. Aharoni, I. Popov and U. Banin, *Angew. Chem., Int. Ed.*, 2006, **45**, 8001; (b) L. Xu, Z. Yin, S.-W. Cao, Z. Fan, X. Zhang, H. Zhang and C. Xue, *Chem. Eur. J.*, 2014, **20**, 2742.

25 (a) J. Yang and J. Y. Ying, *Angew. Chem., Int. Ed.*, 2011, **50**, 4637; (b) J. Yang and J. Y. Ying, *J. Am. Chem. Soc.*, 2010, **132**, 2114.

26 Y. Li, L. Li, Y. Gong, S. Bai, H. Ju, C. Wang, Q. Xu, J. Zhu, J. Jiang and Y. Xiong, *Nano Res.*, 2015, **8**, 3621.

27 D. Seo, C. I. Yoo, J. Jung and H. Song, *J. Am. Chem. Soc.*, 2008, **130**, 2940.

28 (a) C. Han, Z. Li, W.-j. Li, S.-l. Chou and S.-x. Dou, *J. Mater. Chem. A*, 2014, **2**, 11683; (b) S. Zhang, W. Li, B. Tan, S. Chou, Z. Li and S. Dou, *J. Mater. Chem. A*, 2015, **3**, 4793.

29 Y. Hwa, C.-M. Park and H.-J. Sohn, *J. Electroanal. Chem.*, 2012, **667**, 24.

30 X. Xu, B. Dong, S. Ding, C. Xiao and D. Yu, *J. Mater. Chem. A*, 2014, **2**, 13069.

31 S. Chen, Y. Xin, Y. Zhou, F. Zhang, Y. Ma, H. Zhou and L. Qi, *J. Mater. Chem. A*, 2014, **2**, 15582.

32 (a) W. Liu, P. Miao, L. Xiong, Y. Du, X. Han and P. Xu, *Phys. Chem. Chem. Phys.*, 2014, **16**, 22867; (b) W. Jin, P. Xu, L. Xiong, Q. Jing, B. Zhang, K. Sun and X. Han, *RSC Adv.*, 2014, **4**, 53543.

33 Q. Kuang and S. Yang, *CrystEngComm*, 2014, **16**, 4940.

34 Q. Cao, R. Che and N. Chen, *Chem. Commun.*, 2014, **50**, 4931.

35 C. Qiu, L. Zhang, H. Wang and C. Jiang, *J. Phys. Chem. Lett.*, 2012, **3**, 651.

36 (a) J. R. Lombardi and R. L. Birke, *J. Phys. Chem. C*, 2008, **112**, 5605; (b) L. Jiang, P. Yin, T. You, H. Wang, X. Lang, L. Guo and S. Yang, *ChemPhysChem*, 2012, **13**, 3932.